atmosphere

MDPI

Article

Sniffing Drones: A Promising Solution for Measuring Railroad Emissions in Urban Environments

Felipe Baglioli and Ricardo H. M. Godoi *

Department of Environmental Engineering, Federal University of Paraná (UFPR), Curitiba 81531-980, PR, Brazil; felipe.baglioli@gmail.com

* Correspondence: rhmgodoi@ufpr.br

Abstract: Locomotive emissions from railroads can particularly impact air pollution, making it crucial to understand their impacts on human health and the environment and develop strategies to reduce them. The potential of drone technology equipped with a "sniffing" system for detecting air pollution emissions is promising and can be a valuable tool for assessing dynamic emissions. This research utilized sensor-equipped drones to measure gaseous emissions from cargo and passenger trains on a railway in Curitiba, Brazil. Reference equipment evaluated the accuracy of NO_2, SO_2, and O_3 concentrations. The results showed that before the passage of trains, the average SO_2 concentration was 20 $\mu g/m^3$, with a maximum concentration of 110 $\mu g/m^3$ detected during transit. The average increase in NO_2 concentrations was from 30 $\mu g/m^3$ to 120 $\mu g/m^3$, and the average increase in O_3 concentrations was from 80 $\mu g/m^3$ to 135 $\mu g/m^3$. The vertical profiles were evaluated before and after the passage of locomotives, indicating an accumulation of pollutants above the railroad. These findings demonstrate the potential of sniffing drones to measure railroad emissions in urban environments. They also highlight the need to regulate emissions from diesel-powered locomotives to minimize atmospheric pollution and its negative impact on public health in emerging and developing countries.

Keywords: drone; air pollution; railroad emissions; electrochemical sensors; environmental monitoring

Citation: Baglioli, F.; Godoi, R.H.M. Sniffing Drones: A Promising Solution for Measuring Railroad Emissions in Urban Environments. *Atmosphere* **2023**, *14*, 865. https://doi.org/10.3390/atmos14050865

Academic Editor: László Bencs

Received: 5 April 2023
Revised: 6 May 2023
Accepted: 10 May 2023
Published: 12 May 2023

1. Introduction

The first Brazilian railroads were built in 1854 to transport coffee beans and sugar cane. Since then, the country has embraced the mode and expanded it. Most Brazilian cities have one-or-more freight or passenger trains. Diesel trains dominate these roadways, thus contributing to urban air pollution. In contrast to other vehicular emissions, air pollution from railroads is not subject to regulation by the National Environmental Council-CONAMA [1,2]. As a result, locomotives primarily use TFM S1800 diesel, which contains 1800 mg/kg of sulfur [3], contributing to emissions of sulfur oxides and other pollutants into the atmosphere. This sulfuric content indicates that exhaust gases from trains may contain high concentrations of sulfur dioxide (SO_2) and hydrogen sulfide (H_2S), but also volatile organic compounds (VOC's), methane (CH_4), nitrogen oxides (NO_X) and ozone (O_3), due to incomplete combustion [4,5].

Measuring railroad emissions in urban environments poses a significant challenge due to the complex and dynamic nature of the surrounding atmosphere. Using fossil fuels on locomotives can contribute to atmospheric pollution, which can become a public health issue. According to Abbasi's research [6], rail traffic does not affect concentrations at open ground-level stations, while underground or enclosed stations can reach ambient air several times. Non-exhaust particle emissions may be hazardous, and enclosed-rail traffic settings should be monitored for high concentrations.

Particle properties, generation methods, and exposure variables, especially rail-transport non-exhaust emissions, must be studied to create effective countermeasures. This situation is particularly concerning given the high demographic density of urban centers, which leads to increased exposure to polluted air, and a greater incidence of cardiovascular problems related to atmospheric pollution [7].

Sensor-equipped drones offer several advantages over traditional measurement techniques, including increased accuracy, mobility, and cost-effectivity. However, direct implementation of this technology presents challenges such as the representativeness of observations, continuous observation needs, and potential sensor exposure to pollution sources. Incorporating data into air quality monitoring systems requires careful technical evaluation and planning to integrate data into air quality monitoring systems to ensure reliable information for improving policy formulation and decision-making.

Emissions from diesel engines, such as locomotives [7,8], are typically linked with three gas pollutants: SO_2, NOx (consisting of NO and NO_2), and volatile organic compounds (VOCs) produced by fossil fuel combustion. In a subsequent reaction, NOx and VOCs react in the presence of sunlight to form O_3. SO_2 is the primary pollutant related to the combustion of sulfur-rich fuels [9].

For human health, exposure to this gas can cause pulmonary activity reduction, eye, nose, and throat irritation, and even premature mortality [10,11]. These problems are predominantly related to the oxidative stress that SO_2 can produce on respiratory system cells [12,13]. On the one hand, NO_2 is dangerous because of a condition named methemoglobinemia. The gas binds to hemoglobin cells in this condition and changes oxygen transport [14]. Symptoms typically related to NO_2 contamination include coughing, wheezing, and breathing difficulty [15]. In addition to these direct effects, NO_2 indirectly impacts human health, influencing tropospheric O_3 concentrations. Photochemical reactions involving both species determine if an area of the atmosphere will act as a source or a sink for O_3 [16,17]. O_3 is a strong oxidant and, similar to SO_2, has a toxic effect on human respiratory cells through oxidative stress [18]. Although O_3 is naturally found in elevated concentrations in the stratosphere, its presence at tropospheric levels qualifies it as a secondary pollutant [10,19–21].

Given the importance of comprehending these gaseous emissions in urban areas, there is a need for a sampling system to directly measure them, as it is only sometimes feasible to utilize stationary sensors atop locomotive smokestacks. In this context, sensor-equipped drones have been used, besides other applications, to evaluate methane sources and sinks, assess volcanic plumes, measure forest burn emissions, monitor urban air quality and atmospheric pollution, detect gas leaks, and monitor methane emissions from landfills [22]. Nevertheless, the applicability of such a system in evaluating railroad emissions has yet to be extensively assessed.

This study aims to evaluate the efficacy of this strategy for measuring SO_2, O_3, and NO_2 emissions using drones over diesel-powered trains in the urban area of Curitiba-Brazil, to understand the impact of railroads on air quality, as these gases are included in the air quality guidelines by the World Health Organization [23]. This investigation presents the concept of 'sniffer drones' for real-time monitoring of moving pollutant sources in urban environments and discusses the challenges associated with this technology.

2. Materials and Methods

2.1. The "Sniffing" System for Railroad Emissions

Using a drone to measure pollutant concentrations requires compact and lightweight sensors. According to Shelekhov et al. [24], measurements of turbulent fluxes and spectra in the urban atmosphere are viable and reasonably accurate using a sensor-equipped DJI Phantom 4 Standard. The authors used a smoothing procedure to study the behavior of the longitudinal and lateral turbulence spectra in the inertial and energy production ranges. The longitudinal and lateral turbulence scales were estimated by the least squares method using the von Karman model as a regression curve. It was shown that the turbulence

spectra obtained with the DJI Phantom 4 Pro and AMK-03 generally coincide, with minor differences observed in the high-frequency region of the spectrum. In the power generation domain, the longitudinal and lateral turbulence scales and their ratios measured by the DJI Phantom 4 Pro and the AMK-03 agree with reasonable accuracy. In the inertial range, the behavior of the turbulence spectra shows that they obey the Kolmogorov–Obukhov "5/3" law. The airship used in this study was the DJI Phantom 3 Standard.

This model weighs 1216 g, including the battery, and can carry up to 1 kg. However, for safety reasons, it is not encouraged for the cargo weight to surpass 700 g. Additionally, flight autonomy can be decreased from 25 to less than 20 min when carrying more than 500 g [25]. Considering that the main differences between this model and the Phantom 3 are not mechanical flight technology nature [26], it was assumed that the latter model is also capable of measuring turbulent quantities.

Per our experimental design, we elected to position the sensors at the airship's center to mitigate the downwash and dilution impacts arising from the drone propellers [27,28]. In this context, three Envea Cairsens microsensors were selected for this study: one detecting SO_2, one for NO_2, and another for the O_3 measurements. These electrochemical sensors are small and have a relatively low cost, allowing the use of multiple sensors in one airship. The average weight is 42 g and includes an internal data logger that can store up to 1212 days of data with a 60 min sampling frequency. Although, considering the objectives of this study, the sampling frequency used was 1 min, meaning that up to 2 days of data could be stored in the internal data loggers [29]. For gaseous measurements, the resolution of the sensors is 1 ppb, meaning that the uncertainty related to measured concentrations is $\pm$0.5 ppb [29]. Considering conversion factors at 25 °C and 1 atm, this uncertainty is $\pm$1.31 $\mu g/m^3$ for SO_2, $\pm$0.98 $\mu g/m^3$ for O_3 and $\pm$0.94 $\mu g/m^3$ for NO_2. The assessment of the cross-sensitivity of the NO_2 and NO_2-O_3 sensors found that the sensor exhibits a response consistent with Cl_2 at levels comprising approximately 80% of the total signal output [30,31]. The study's accuracies are founded upon the performance that manufacturers have claimed. Data measured with this equipment was treated by an outlier removal process described by Junior and Dias [32].

One disadvantage of the Cairsen sensors is the lack of an internal battery, which demands an external energy feed. Also, due to the electrochemical principle used in these sensors, sharing their energy source with the drone could induce some noise in measured datasets [33]. For this reason, the drone was equipped with a small power bank connected to a USB hub. This way, the power bank had enough power to charge three sensors for up to 5 days. The energy consumption of these sensors is low, staying close to 15 mA at 5 VDC [29]. Considering the weight of the power bank, USB hub, and sensors, this configuration made the total cargo on the airship reach 218 g. This value is lower than the 500 g threshold for maintaining flight autonomy over 20 min without jeopardizing the safety of flights.

The authors conducted test flights with the assembled equipment to establish guidelines and strategies for the sampling flights. First, the flight guidelines [34] included the respect of regulations from the Brazilian Civil Aviation National Agency (ANAC) concerning flight speeds, drone operations, and distance from non-consenting people and animals. Additional constraints were incorporated into the guidelines to ensure the safety and maximize the effectiveness of the sampling flights. These constraints consider meteorological factors, such as wind speed, precipitation, visibility, and other related variables that may pose a risk to the operation.

Our study established that sampling flights were not conducted during periods of precipitation or high wind velocity due to the potential impact of these meteorological conditions on the measurements' accuracy. Our study established a protocol whereby the drone must land as soon as possible while maintaining a safe distance from non-consenting third parties if the pilot observed any meteorological conditions during a flight. This precaution was necessary due to the potential for abrupt changes in meteorological conditions during measurement, which could reduce the number of actual measurements

obtained and impede continued data collection. The relatively light weight of the drone increased its susceptibility to becoming uncontrollable in high wind conditions, posing potential risks. On days deemed suitable for sampling flights, our measurement protocol dictated assessing background concentrations and emission plumes. Prior to train passage, the airship was positioned approximately 5 m above the railroad for a 15 min period, during which background concentrations were sampled. The collected data were then analyzed, with the mean values obtained for each pollutant serving as the reference point for the corresponding day. When the train was observed, take-off operations commenced. The drone was positioned at an average effective emission height of approximately 5 m above the railroad, a height chosen after considering the locomotives under study. As the train passed, the airship was slowly elevated to the upper limit of the visible emission plume before returning to its initial height of 5 m, where it remained stationary for an additional 10 min period following the train's passage. This method facilitated the examination of gas concentration effects during pre-, intra-, and post-locomotive pass-by periods, providing a comprehensive evaluation of railroad emission impacts.

To provide additional assessment, the team constructed vertical profiles of SO_2, NO_2, and O_3 above the railroad. These profiles were obtained over point 1 (details in Section 2.2) before and 5 min after passing a passenger train. For them, the drone was programmed to start sampling about 1 m above railroad level, measuring for 1 min for each meter. Therefore, the vertical resolution for these profiles was 1 m. Then, after reaching a height of 15 m, the drone was returned to the landing platform. The measured profiles were short, characterizing only a tiny part of the atmosphere above the railroad. However, due to the battery autonomy of the airship, the most extended possible profiles were 15 m in height without compromising the safety of the flights.

2.2. Area of Study

The authors selected the study area in Curitiba (PR), shown in Figure 1, based on three primary considerations: proximity to the laboratory at UFPR for easy equipment transportation, availability of a suitable take-off and landing platform (green area in Figure 1), and the presence of numerous points of interest. These sites include residential blocks near the railroad (yellow triangle). This religious institution aids the socially vulnerable (blue triangle), and the Marcelino Champagnat Hospital provides cardiovascular treatments (red cross). Furthermore, the authors considered a bike lane beside the railroad approximately 5 m above the ground (blue line).

The selected area had two sampling points: point 1 and point 2, which are shown as green and red triangles, respectively, in Figure 1. Point 1 was defined as the sampling point for measures over the smokestacks. As mentioned, the effective emission height was set at an average of 5 m above the railroad line. This way, that height was defined as the starting height of point 1, allowing it to be used on direct emission sampling flights.

On certain days, meteorological conditions proved unsuitable for conducting sampling flights. In such cases, point 2 was used for data collection. This designated location is above the bike path adjacent to the rail line, approximately 6 m above the level of the rail line. It represents the average train nose level for a passerby on the bike path. This selection was made to assess the impact of railroad emissions on nearby areas. Notably, the measurements at point 2 were not made with an airship, but the drone remained on the ground with the power off. Since meteorological measurements were unavailable at the site, trained personnel made local and intuitive assessments based on various considerations, such as visual observation of cloud cover and wind speed, assessment of temperature and humidity, and review of weather forecasts from nearby regions. While the data collected at point 2 provides valuable insights into the effects of railroad emissions on nearby areas, it is crucial to interpret the results with caution due to the potential influence of overestimation or underestimation of actual values.

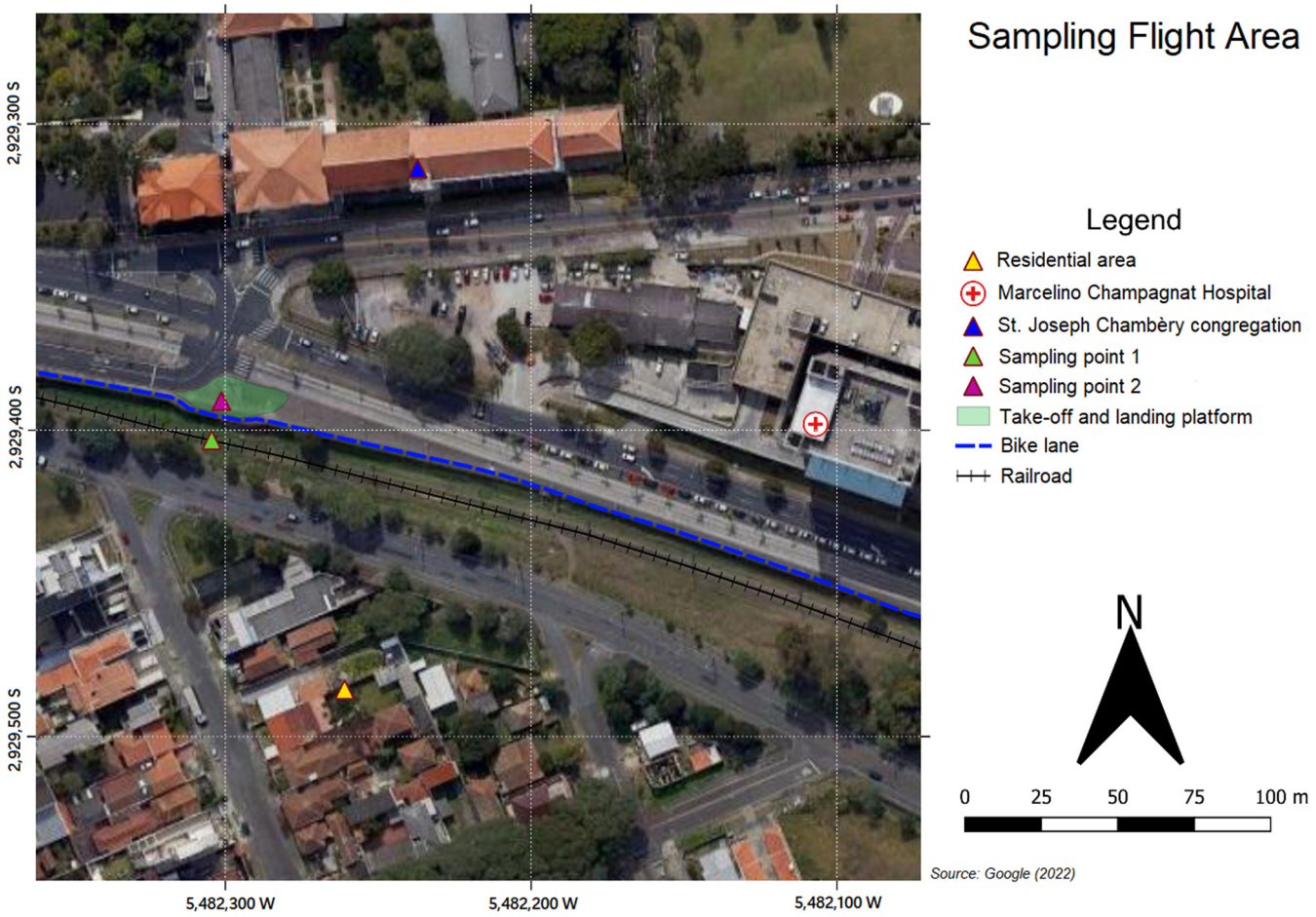

Figure 1. Area used for sampling flights. Source: [35].

During this study, the authors conducted eight sampling campaigns to measure pollutant concentrations at various points in the study area. Most sampling flights (five campaigns) were performed at point 1, with the final campaign occurring on December 25th to determine the vertical profiles of pollutant concentrations at this location. Adverse meteorological conditions resulted in two campaigns being carried out at point 2. Outliers were removed from the measured data, and the datasets were evaluated for each gaseous substance, as shown in Sections 3.1–3.3. In these sections, captions were added to the graphs to facilitate comprehension. Measurements made at sampling point one were labeled as SP 1. Meanwhile, tag SP 2 was used over measurements made on sampling point 2. Moreover, cargo trains were labeled with the letter C, and passenger trains with the letter P. Afterwards; Section 3.4 includes the results for the vertical profiles, both before and after the passage of the passenger train.

3. Results

3.1. Sulfur Dioxide

On different days, the measured background concentrations of SO_2 ranged from 10 $\mu g/m^3$ and 30 $\mu g/m^3$. After the passing of locomotives, in all the campaigns, absolute increases varying from 16 $\mu g/m^3$ and 114 $\mu g/m^3$ concentration were observed, as shown in Figure 2. The values shown in the dark blue bars represent the maximum value observed during each sampling flight.

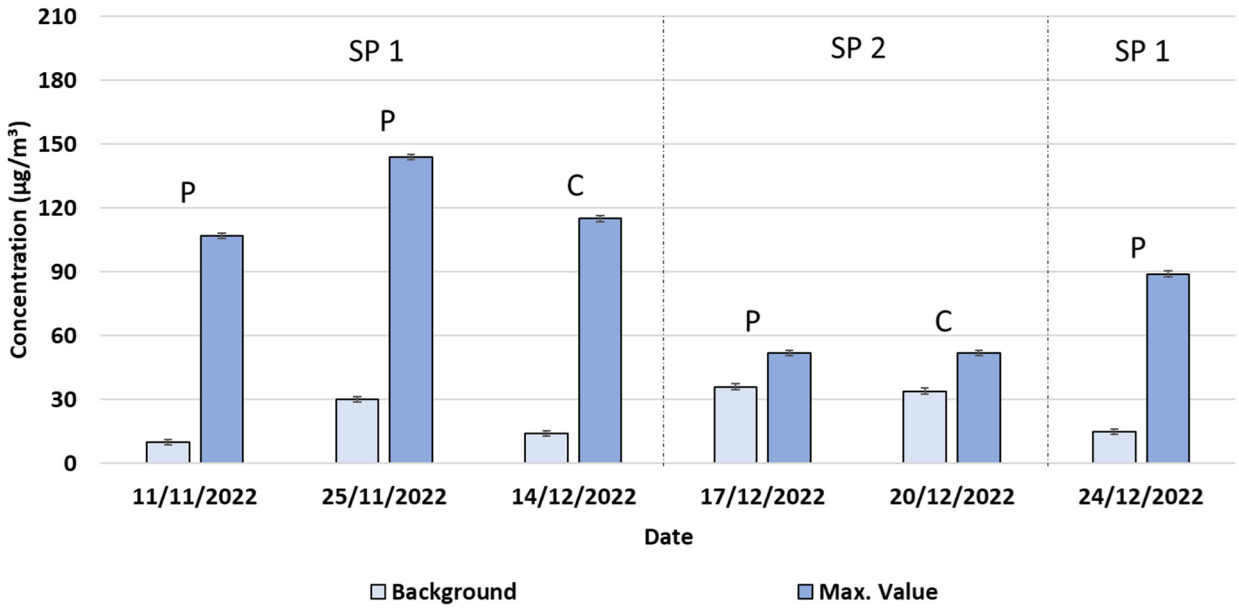

Figure 2. Background and maximum concentrations of SO_2 measured during sampling flights. Cargo trains are indicated with the letter C, while passenger trains are indicated with the letter P. SP 1 means measurements over sampling point 1, and SP 2 is related to sampling point 2.

Although the highest absolute increase, 114 µg/m^3, was observed after a passenger train on November 25, relative increases did not change between passenger trains when separately comparing the two-sampling point. In point 1, the relative increase fluctuated around 600%, while at point 2, it was much lower at around 40%. The SO_2 concentration increases measured at point 2 during train passage were considerably lower than point 1. In addition, the difference between cargo and passenger train emissions at point 2 was slight at 2 µg/m^3 and close to the sensor's uncertainty. For most campaigns, maximum concentrations of SO_2 were observed at the same time as the passage of the locomotive. Moreover, in both SP 1 and SP 2, the maximum values of SO_2 during train passage exceeded the DQA established by the WHO.

3.2. Ozone

As presented in Figure 3, O_3 background concentrations showed high variability in different campaigns. Average values as low as 30 µg/m^3 and as high as 60 µg/m^3 were measured during the sampling flights. Even with this high variability, the passage of trains elevated the levels of O_3 consistently in every campaign, with a relative increase over SP 1 in the order of 200%. Differently from what was noted for SO_2, the absolute increase in O_3 concentrations was higher for cargo trains compared to their passenger counterparts. While passenger trains caused a maximum absolute increase in O_3 concentration of 77 µg/m^3, cargo trains' absolute increase was over 120 µg/m^3 in both measured cases. This was especially true for the measurements at point 2, where the total increase was almost two times higher during the passage of a cargo train than the observed increase after the passenger train.

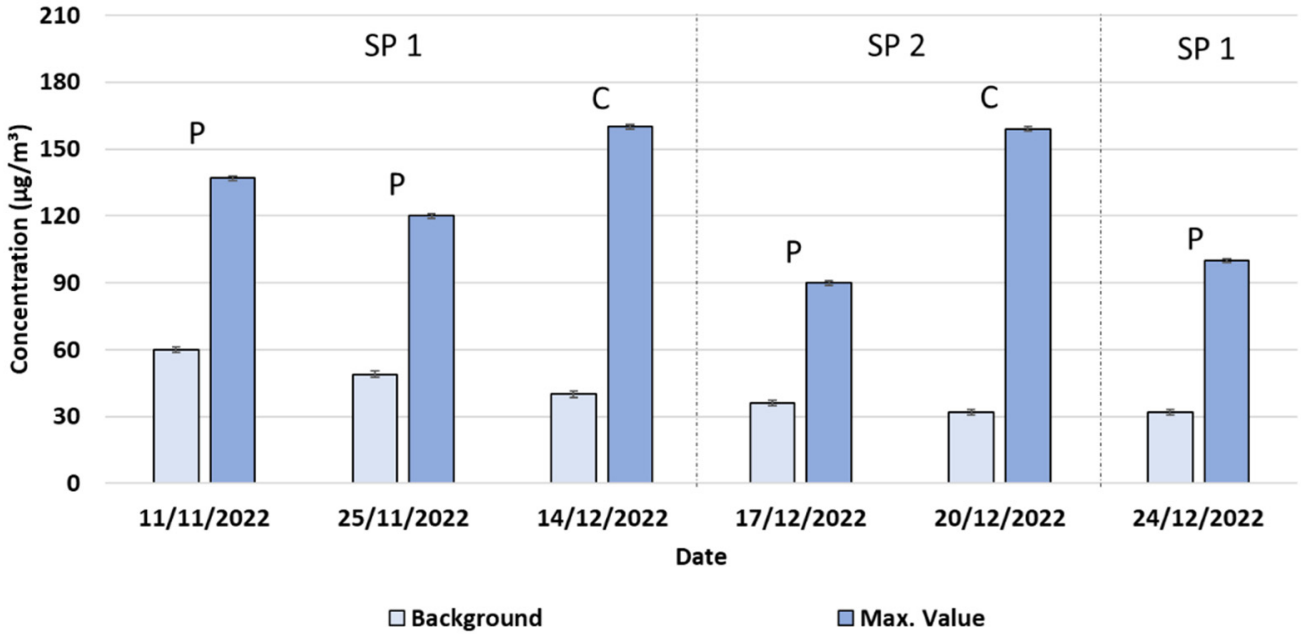

Figure 3. Background and maximum concentrations of O_3 were measured during sampling flights. Cargo trains are indicated with the letter C, while passenger trains are indicated with the letter P. SP 1 means measurements over sampling point 1, and SP 2 is related to sampling point 2.

Furthermore, maximum concentrations were regularly observed 3 to 4 min after the passage of the trains. This time lag can be related to the secondary nature of O_3 in the troposphere, as shown in Section 2, thus the highest O_3 concentrations were observed after the locomotives passed.

3.3. Nitrogen Dioxide

In contrast to what was observed for background values of SO_2 and O_3, it was found that the average concentrations obtained for NO_2 were more uniform in different campaigns. The background values of NO_2 concentration stayed between 25 µg/m^3 and 30 µg/m^3. In addition, increases in these background values were observed during train passage on all campaigns, Figure 4. An analysis of the NO_2 emissions from the cargo and passenger trains at multiple sampling points reveals notable differences in absolute increases. On SP 1, most of the measured passenger trains caused an absolute increase in the order of 85 µg/m^3. In contrast, the cargo train passage was followed by an absolute increase of 140 µg/m^3 in NO_2 concentration.

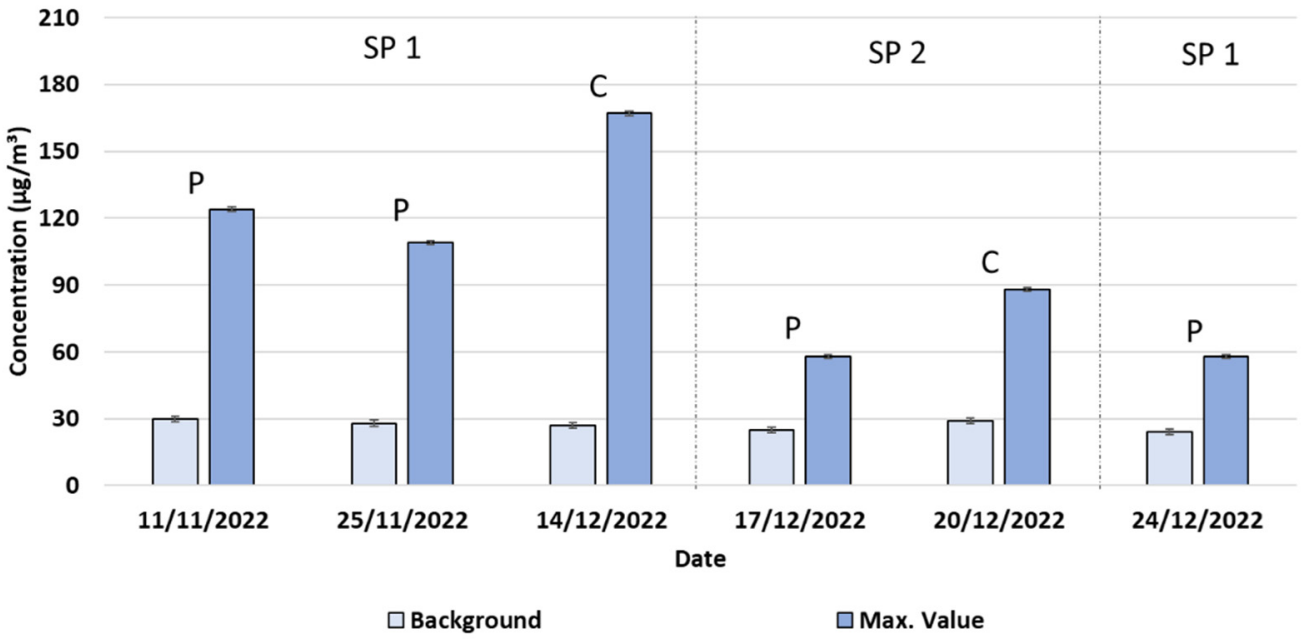

Figure 4. Background and maximum concentrations of NO_2 were measured during sampling flights. Cargo trains are indicated with the letter C, while passenger trains are indicated with the letter P. SP 1 means measurements over sampling point 1, and SP 2 is related to sampling point 2.

Specifically, cargo trains exhibit absolute increases in the concentrations of NO_2, almost twice higher than passenger trains. The maximum values measured at SP 2, 58 $\mu g/m^3$ and 88 $\mu g/m^3$, indicate that our findings show that areas close to railroad tracks are particularly vulnerable to elevated concentrations of NO_2 emissions. As well as O_3 concentrations, maximum NO_2 values were measured roughly 2 min after the passage of the trains. This time lag was consistent during every sampling campaign.

3.4. Vertical Profiles

As discussed in Section 2, the sampling flights on December 25 were used to construct vertical profiles of gaseous concentrations over point 1. These profiles were measured for SO_2, O_3, and NO_2, beginning about 1 m above railroad level and ending about 15 m above railroad level.

The first three profiles in Figure 5 represent the atmospheric concentrations of SO_2, O_3, and NO_2, in purple, without the passage of a locomotive. By examining these profiles, the authors can gain insight into the background levels of these gasses before trains pollute the environment. It is noted that concentrations are more than 20 $\mu g/m^3$ higher than the guidelines stipulated by the WHO for the former and more than 5 $\mu g/m^3$ higher for the latter. It is important to emphasize that rigorously measured concentrations cannot be directly compared to the AQGs, since these are defined as 24 h or 8 h averages for the considered gases. However, they can be treated as reference values and are therefore utilized as such in this paper.

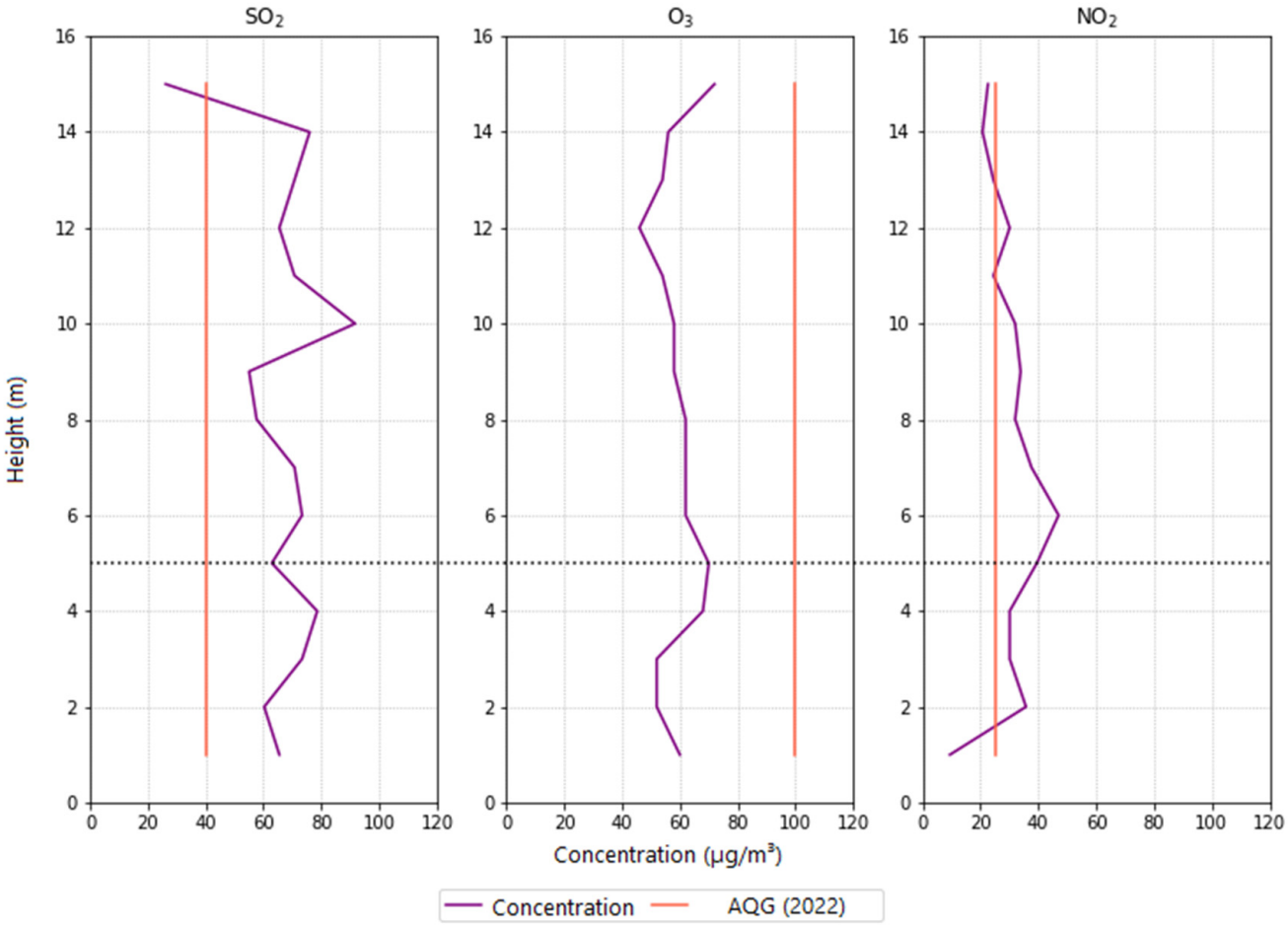

Figure 5. Vertical profiles of SO_2, O_3 and NO_2 measured over the railroad before the passage of a passenger train. In orange, the air quality guideline defined by the WHO for each pollutant.

Moreover, a minor O_3 and NO_2 accumulation with concentrations reaching up to 47 µg/m^3 can be seen near the smokestack level, 5 m above the railroad level (Figure 5 as the dotted line). This accumulation cannot be seen for SO_2. Instead, concentrations of this pollutant tend to accumulate between 10 m and 14 m above the railroad level, with values reaching 90 µg/m^3.

Shortly after 8:30 a.m. local time, a passenger train passed sampling point 1. About 5 min after this passage, the sniffing drone was deployed, measuring the vertical profile of gaseous concentrations one more time. These profiles are presented in Figure 6. In addition, Figure 6 contains the average peak concentrations of each gas measured during passenger train passages, represented by the red dots: 105 µg/m^3 for SO_2, 128 µg/m^3 for O_3, and 116 µg/m^3 for NO_2. The concentrations after the train increased for each pollutant throughout the vertical profile. The maximum increase observed for SO_2 occurred at the height of 10 m, from 90 µg/m^3 prior to the train passage to 152 µg/m^3. In addition, concentrations of O_3 and NO_2 were higher near the stack, reaching 108 µg/m^3 for the prior and 74 µg/m^3 for the latter. In contrast, SO_2 concentrations were higher at 7 and 10 m altitude.

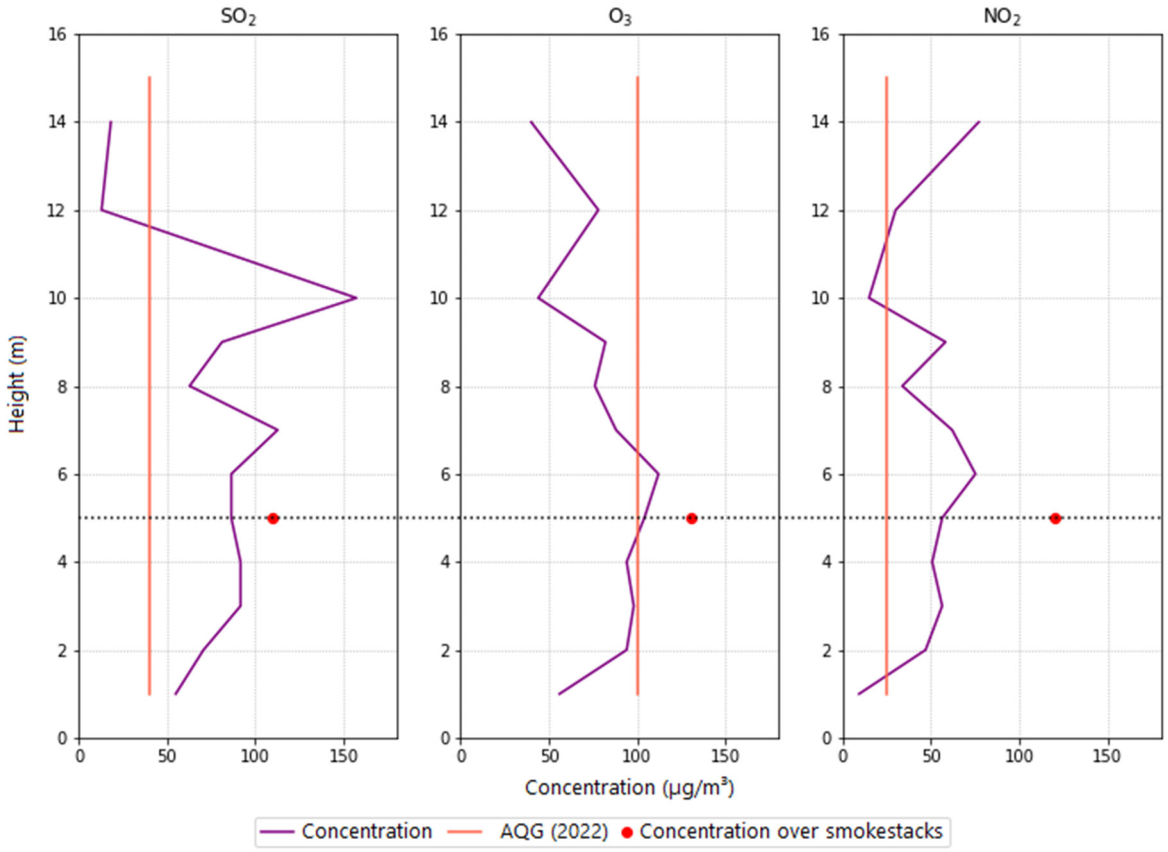

Figure 6. Vertical profiles of SO_2, O_3, and NO_2 were measured 5 min after a passenger train passed over the rail line. The red dots represent the mean concentration measured over the smokestacks of passenger trains. In orange, the WHO defines the air quality guideline for each pollutant.

In addition to the higher concentration values, the profiles in Figure 6 reveal the height of the locomotive's emission plume 5 min after its passage. According to the SO_2 profile, above 10 m, concentrations of SO_2 decrease rapidly. Similarly, the O_3 and NO_2 concentrations are proportionate up to 10 m. This behavior suggests that 5 min after a passenger train passes, the emission plume reaches a height of 10 m. Above this height, this relationship is no longer evident.

4. Discussion

The evaluation was limited to two cargo trains, while four passenger trains were assessed. The goal of comparing these types of trains was to determine which emitted higher atmospheric pollutants. This assumption was based primarily on the fact that cargo trains passing through the area of interest are typically longer and heavier than passenger trains and therefore require more fuel consumption, which leads to higher concentrations of the gases being studied. During the sampling campaigns conducted for this study, the presence of passing cargo trains in the study region presented a challenge. Unlike passenger trains, whose departure times are publicly available and easily accessible, cargo train schedules are confidential and can vary significantly on different dates. As a result, acquiring emissions data from cargo trains required more time and effort. This was true for the NO_2 concentrations and even more so for O_3 concentrations. In the latter case, absolute increases in concentration were more significant after the passage of cargo trains for measurements made at both point 1 and point 2. The total increase at point 2 due to the passage of a cargo train was almost twice as significant as the increase due to the passage of a passenger train.

Contrary to this, no substantial numerical differences in SO_2 concentrations were observed. Increases in SO_2 from passenger and cargo trains were not distinguishable. Due to the high sulfur content of locomotive fuels, it is plausible that SO_2 emissions will remain high despite a decrease in cargo loads and fuel consumption. However, it also suggests that O_3 and NO_2 emissions may be more dependent on the weight of the trainload.

Increases in SO_2 from the passenger and cargo trains were not significantly different, and SO_2 emissions may remain substantial even as cargo loads and fuel usage decrease due to the high sulfur content of locomotive fuels. Thus, O_3 and NO_2 emissions could be more sensitive to the train's cargo weight. The authors can draw analogous arguments by comparing the measurements collected at sample sites 1 and 2. Consistent with our expectations, higher concentration increases were observed more frequently at point 1, directly over the smokestacks. However, the authors also observed different behaviors on sampling point 2, with small absolute increases in gaseous concentration being the norm. We attribute this to the high temperatures at which the exhaust gases from the smokestacks are produced, causing them to rise rapidly in the atmosphere so that there is not enough time for the elevated concentrations to reach the nose of the train on the side of the railroad.

These findings suggest that the impact of railroad emissions on surrounding areas is insignificant compared to the impact on the railroad itself. The authors confirm this assumption by noting the similarity between the O_3 amounts measured at points 1 and 2. The influence of emission temperature on O_3, which acts as a secondary pollutant, is comparatively smaller than that on primary gases. Substantial O_3 concentrations can be measured even at passerby's nose levels on the railroad's side during the locomotives' passage. These results represent the first emissions data obtained from moving trains using a drone. They are the starting point for understanding the spatial distribution of railroad emissions and their potential impact on air quality in the research area.

Acquisition of vertical profiles of contaminant concentrations has provided valuable insight into the circumstances of the investigation. By comparing gas profiles before and after train passage, the authors confirmed that railroad emissions could indeed increase concentrations of SO_2, NO_2, and O_3 in the atmosphere of surrounding communities. In addition, it is important to emphasize that due to the lack of legislation, direct comparisons with the World Health Organization's air quality guidelines (WHO) are not possible in our study because the authors do not have 24 h estimates. Nevertheless, our studies have provided preliminary evidence that these parameters are exceeded. The authors observed that these gases accumulate in the lower atmosphere before a train passes, leading to concentrations that immediately exceed the AQGs in 75% for SO_2 and 25% for NO_2. It is worth noting that this does not necessarily indicate that the air quality in the research area is poor, but it does indicate a deterioration in air quality. Our findings have significant implications for policymakers and stakeholders, who must consider the impact of railroad emissions on nearby communities and the environment.

5. Conclusions

This study presents preliminary findings through eight sampling campaigns conducted in Curitiba, Brazil. The measurement technique employed in this study involves sampling both background concentrations and locomotive emission plumes of SO_2, O_3, and NO_2. As part of our study, eight sampling campaigns were conducted using a drone equipped with Envea Cairsen microsensors to accurately measure pollutant concentrations at various locations in the research area. The results demonstrate the efficacy of using compact and lightweight microsensors mounted on drones to assess the impact of train emissions on ambient air quality. Measurements taken before and after the trains passed showed increases in all three pollutants, with the most significant increase in SO_2 after passenger trains and O_3 after cargo trains. NO_2 concentrations were also higher after the cargo trains, even near the railroad. Maximum concentrations were observed 2–4 min after train passage. While drones equipped with sensors have demonstrated the ability to detect locomotive pollution, the accuracy of these measurements can be influenced

by wind speed and direction; however, implementing microsensors as anemometers on drones in the future will facilitate the detection of weather changes leading to more accurate pollution sensing.

This investigation underscores the importance of monitoring air pollution from transportation sources and proposes a potential solution for achieving this aim. Leveraging drones and lightweight sensors can substantially aid in comprehending and mitigating the impact of transportation emissions on air quality and public health. The findings of this study are valuable for policymakers and transportation authorities in devising strategies to counteract the detrimental effects of railroad transportation on air quality. Further research is necessary to validate and generalize these findings to other regions.

Author Contributions: Both authors contributed equally and integrally to the development of the research and the presentation of the results. All authors have read and agreed to the published version of the manuscript.

Funding: This research received no external funding.

Data Availability Statement: No new data was created during the study, and no relevant publicly available datasets exist for this research.

Conflicts of Interest: The authors declare no conflict of interest.

References

1. Conselho Nacional do Eeio Ambiente (CONAMA). *Resolução Conama no 18, de 06/05/1986. Dispõe Sobre a Criação do Programa de Controle de Poluição do ar Por Veículos Automotores—PROCONVE*; Ministério do Meio Ambiente (MMA): Brasília, Brazil, 1986.
2. Conselho Nacional do Eeio Ambiente (CONAMA). *Resolução Conama no 315, de 29/10/2002. Dispõe Sobre a Nova Fase do Programa de Controle de Poluição do ar Por Veículos Automotores—PROCONVE*; Ministério do Meio Ambiente (MMA): Brasília, Brazil, 2002.
3. Petrobras. *Óleo Diesel: Informações Técnicas*, 1st ed.; 2021; p. 26. Available online: https://petrobras.com.br/data/files/04/93/72/4C/5A39C710E2EF93B7B8E99EA8/Manual-de-Diesel_2021.pdf (accessed on 22 August 2022).
4. Paralovo, S.L. Análise de Poluentes Gasosos e Material Particulado Fino Em Manacapuru, AM. Master's Thesis, Federal University of Paraná, Curitiba, Brazil, 2016.
5. Zanella, T.V. Navios e poluição do ar: Um estudo sobre a regulação das emissões atmosféricas por embarcações. *Rev. Esc. Guerra Nav.* **2018**, *24*, 301–328. [CrossRef]
6. Abbasi, S.; Jansson, A.; Sellgren, U.; Olofsson, U. Particle Emissions from Rail Traffic: A Literature Review. *Crit. Rev. Environ. Sci. Technol.* **2013**, *43*, 2511–2544. [CrossRef]
7. Mir, S.A.; Bhat, J.I.; Lone, F.; Rehman, M.U.; Nazir, N.; Lone, A.A.; Ali, T.; Jehangir, A. Synergistic effects of vehicular emissions (NO_2, SO_2 and SPM) on progression of *Crocus sativus* L. in saffron bowl kashmir. *Adv. Environ.* **2021**, *3*, 100033. [CrossRef]
8. D'agosto, M.d.A. *Transporte, Uso de Energia e Impactos Ambientais: Uma Abordagem Introdutória*, 1st ed.; Elsevier: Rio de Janeiro, Brazil, 2015; p. 251, ISBN 978-85-352-2821-2.
9. EPA. Sulfur Dioxide Basics. United States Environmental Protection Agency. 2022. Available online: https://www.epa.gov/so2-pollution/sulfur-dioxide-basics (accessed on 15 June 2022).
10. EPA. Health Effects of Ozone Pollution. United States Environmental Protection Agency. 2022. Available online: https://www.epa.gov/ground-level-ozone-pollution/health-effects-ozone-pollution (accessed on 22 August 2022).
11. World Bank. *Pollution Prevention and Abatement Handbook: Toward Cleaner Production*; The International Bank for Reconstruction and Development: Washington, DC, USA, 1999; p. 472. ISBN 0-8213-3638-x.
12. Di Meo, S.; Reed, T.T.; Venditti, P.; Victor, V.M. Role of ROS and RNS sources in physiological and pathological conditions. *Oxid. Med. Cell. Longev.* **2016**, *12*, 1245049. [CrossRef]
13. Reno, A.L.; Brooks, E.G.; Ameredes, B.T. Mechanisms of heightened airway sensitivity and responses to inhaled SO_2 in asthmatics. *Environ. Health Insights* **2015**, *9*, 13–25. [CrossRef] [PubMed]
14. Gaston, B.; Drazen, J.M.; Loscalzo, J.; Stamler, J.S. The biology of nitrogen oxides in the airways. *Am. J. Respir. Crit. Care Med.* **1994**, *149*, 538–551. [CrossRef]
15. EPA. Basic Information about NO_2. United States Environmental Protection Agency. 2022. Available online: https://www.epa.gov/no2-pollution/basic-information-about-no2 (accessed on 22 August 2022).
16. Seinfeld, J.H.; Pandis, A.N. *Atmospheric Chemistry and Physics: From Air Pollution to Climate Change*, 2nd ed.; John Wiley & Sons: Hoboken, NJ, USA, 2006; p. 1248. ISBN 978-0-471-72018-8.
17. Nguyen, D.-H.; Lin, C.; Vu, C.-T.; Cheruiyot, N.K.; Nguyen, M.K.; Le, T.H.; Lukkhasorn, W.; Vo, T.-D.; Bui, X.-T. Tropospheric ozone and NOx: A review of worldwide variation and meteorological influences. *Environ. Technol. Innov.* **2022**, *28*, 102809. [CrossRef]

18. Chen, T.-M.; Kuschner, W.G.; Gokhale, J.; Shofer, S. Outdoor air pollution: Ozone health effects. *Am. J. Med. Sci.* **2007**, *333*, 244–248. [CrossRef] [PubMed]
19. CCAC. Tropospheric Ozone: Climate & Clean Air Coalition. 2022. Available online: https://www.ccacoalition.org/en/slcps/tropospheric-ozone (accessed on 22 August 2022).
20. EPA. Basic Ozone Layer Science. United States Environmental Protection Agency. 2021. Available online: https://www.epa.gov/ozone-layer-protection/basic-ozone-layer-science#:~:text=the%20ozone%20layer%20lies%20approximately,earth\T1\textquoterights%20surface%2c%20in%20the%20stratosphere (accessed on 15 September 2022).
21. EPA. Ground-Level Ozone Basics. United States Environmental Protection Agency. 2022. Available online: https://www.epa.gov/ground-level-ozone-pollution/ground-level-ozone-basics (accessed on 3 November 2022).
22. Jońca, J.; Pawnuk, M.; Bezyk, Y.; Arsen, A.; Sówka, I. Drone-Assisted Monitoring of Atmospheric Pollution—A Comprehensive Review. *Sustainability* **2022**, *14*, 11516. [CrossRef]
23. WHO. Air Quality and Health. World Health Organization. 2021. Available online: https://www.who.int/teams/environment-climate-change-and-health/air-quality-and-health/health-impacts (accessed on 17 June 2022).
24. Shelekhov, A.; Afanasiev, A.; Shelekhova, E.; Kobzev, A.; Tel'minov, A.; Molchunov, A.; Poplevina, O. Low-Altitude Sensing of Urban Atmospheric Turbulence with UAV. *Drones* **2021**, *6*, 61. [CrossRef]
25. DJI. Phantom 3 Standard Specifications. 2022. Available online: https://www.dji.com/br/phantom-3-standard (accessed on 14 June 2022).
26. DJI. Phantom 3 (Pro) Vs. Phantom 4 (Pro): Review of the Image Quality Comparison. 2023. Available online: https://store.dji.com/guides/phantom-3-pro-vs-phantom-4-pro-image-quality/ (accessed on 3 March 2023).
27. Brinkman, J.L.; Davis, B.; Johnson, C.E. Post-movement stabilization time for the downwash region of a 6-rotor uav for remote gas monitoring. *Heliyon* **2020**, *6*, 9. [CrossRef]
28. Roldán, J.J.; Joossen, G.; Sanz, D.; Del Cerro, J.; Barrientos, A. Mini-UAV based sensory system for measuring environmental variables in greenhouses. *Sensors* **2015**, *15*, 3334–3350. [CrossRef] [PubMed]
29. ENVEA. Miniature Solution for Real-Time Continuous Pollution Monitoring. France. 2022. Available online: https://www.envea.global/design/medias/envea_cairsens_air-quality-odors-microsensors_en.pdf (accessed on 22 August 2022).
30. Spinelle, L.; Gerboles, M.; Aleixandre, M. *Report of the Laboratory and In-Situ Validation of Micro-Sensors for Monitoring Ambient Air Pollution-O12: CairClipO_3/NO_2 of CAIRPOL (F). EUR 26373*; JRC86479; Publications Office of the European Union: Luxembourg, 2013.
31. Spinelle, L.; Gerboles, M.; Aleixandre, M. *Report of Laboratory and In-Situ Validation of Micro-Sensor for Monitoring Ambient Air Pollution-NO9: CairClipNO_2 of CAIRPOL (F). EUR 26394*; JRC86499; Publications Office of the European Union: Luxembourg, 2013.
32. Junior, D.V.; Dias, N.L. Método Empírico para Determinação de Outliers em Séries de Fluxos de Dados Micrometeorológicos Pós-processados. *Ciência Natura* **2013**, *35*, 150–152.
33. Gu, Q.; Michanowicz, D.R.; Jia, C. Developing a modular unmanned aerial vehicle (UAV) platform for air pollution profiling. *Sensors* **2018**, *18*, 4363. [CrossRef]
34. Ministério da Defesa. *Aeronaves não Tripuladas para uso Recreativo—Aeromodelos*; Comando da Aeronáutica. MCA 56-2; Ministério da Defesa: Brasília, Brazil, 2020.
35. Google. Curitiba. 2021. Available online: https://www.google.com.br/maps (accessed on 29 December 2022).